

Comparison of Kinetic Theory and Hydrodynamics for Poiseuille Flow

Yihao Zheng*, Alejandro L. Garcia[†] and Berni J. Alder[†]

*Department of Applied Science, University of California, Davis CA 95616

[†]Center for Applied Scientific Computing, Lawrence Livermore National Laboratory, Livermore, CA 94551

Abstract. Comparison of particle (DSMC) simulation with the numerical solution of the Navier-Stokes (NS) equations for pressure-driven plane Poiseuille flow is presented and contrasted with that of the acceleration-driven Poiseuille flow. Although for the acceleration-driven case DSMC measurements are qualitatively different from the NS solution at relatively low Knudsen number, the two are in somewhat better agreement for pressure-driven flow.

INTRODUCTION

The hydrodynamic equations may be obtained as a first approximation to the Boltzmann equation [1] and are generally accurate at the macroscopic level except under some extreme conditions [2, 3], since these Navier-Stokes equations, are derived under the assumptions of local equilibrium, small gradients and flows with small Knudsen number. Surprisingly, even for the simple case of acceleration-driven Poiseuille flow with relatively small gradients and Knudsen number, the Navier-Stokes equations fail to give qualitatively correct predictions. Specifically, they fail to reproduce the central minimum in the temperature profile and a non-constant pressure profile, which are both predicted by kinetic theory and observed in numerical simulations down to Knudsen numbers of 10^{-2} . [4]-[11] Furthermore, it is not possible to correct this failure by modifying the equation of state, transport coefficients or boundary conditions and, unlike slip phenomena, the discrepancy is not just near a boundary but throughout the system. The object of this paper is to investigate whether a similar discrepancy occurs in what appears to be an equivalent system, namely pressure-driven Poiseuille flow.

The Navier-Stokes equations have the following form [12]:

$$\frac{\partial \rho}{\partial t} + \nabla \cdot (\rho \mathbf{v}) = 0 \quad (1)$$

$$\rho \left[\frac{\partial \mathbf{v}}{\partial t} + (\mathbf{v} \cdot \nabla) \mathbf{v} \right] = \rho \mathbf{f} - \nabla p + \nabla \cdot \mu \nabla \mathbf{v} + \frac{1}{3} \nabla (\mu \nabla \cdot \mathbf{v}) = \rho \mathbf{f} - \nabla \cdot \mathbf{P}_{ij} \quad (2)$$

$$\rho c_v \left[\frac{\partial T}{\partial t} + (\mathbf{v} \cdot \nabla) T \right] = \nabla \cdot (\kappa \nabla T) + \Phi - p \nabla \cdot \mathbf{v}, \quad (3)$$

where ρ is density, \mathbf{v} velocity, \mathbf{f} body force acceleration, \mathbf{P}_{ij} pressure tensor, p pressure, μ viscosity, c_v heat capacity, κ thermal conductivity, and Φ the dissipation function (i.e. viscous heating). Pressure-driven flow is related to the acceleration-driven case because a constant gradient of pressure will serve as a constant body force (acceleration), that is, the first two terms on the right hand side of eqn. (2) are equivalent at the hydrodynamic level. At the microscopic level the two driving forces are very different since an external force accelerates individual particles while a pressure gradient induces a collective flow due to a spatial variation of the particles. For acceleration-driven Poiseuille flow only the first two terms on the right hand side of eqn. (3) contribute but for pressure-driven flow there can also be cooling by expansion when the flow is compressible (i.e., when $\nabla \cdot \mathbf{v} \neq 0$).

In this paper the velocity, temperature, pressure, pressure tensor and heat flux profiles are obtained from DSMC simulations for both acceleration-driven and pressure-driven Poiseuille flows and compared with numerical solutions

of the Navier-Stokes equations. In hydrodynamics, the pressure tensor [13] can be expressed by

$$\mathbf{P}_{ij} = p\delta_{ij} - \tau_{ij}, \quad (4)$$

where τ_{ij} represents the viscous stress tensor given by

$$\tau_{ij} = \mu \left[\left(\frac{\partial v_i}{\partial x_j} + \frac{\partial v_j}{\partial x_i} \right) - \frac{2}{3} \delta_{ij} \frac{\partial v_k}{\partial x_k} \right] \quad (5)$$

where i, j, k are x, y or z with implied summation over k . The heat flux is defined as $\mathbf{q} = -\kappa \nabla T$. In DSMC simulation, the corresponds quantities are defines as [9]

$$\mathbf{P}_{ij} = \langle m \mathbf{c}_i \mathbf{c}_j \rangle - \rho \mathbf{v}_i \mathbf{v}_j \quad (6)$$

$$\mathbf{q}_i = \frac{1}{2} \langle m \mathbf{c}_i \mathbf{c}^2 \rangle - \langle m \mathbf{c}_i \mathbf{c}_k \rangle \mathbf{v}_k + \rho \mathbf{v}_i \mathbf{v}^2 - \frac{1}{2} \mathbf{v}_i \langle m \mathbf{c}^2 \rangle \quad (7)$$

where \mathbf{c} is the particle velocity, i, j, k are x, y or z with implied summation over k . The angle brackets define volume averages over particles with

$$\rho = \langle m \rangle \quad \mathbf{v} = \langle m \mathbf{c} \rangle / \rho \quad (8)$$

In the next section the numerical schemes for the Navier-Stokes solver and the DSMC simulations are described. The following section presents the results of the numerical investigations. The paper concludes with a discussion of our results and a list of further directions are given.

POISEUILLE FLOW

In Poiseuille flow the fluid is confined between two rigid parallel plates that are stationary and act as thermal reservoirs. In the acceleration-driven case the boundary conditions are taken as periodic in the flow direction and a constant body force is applied in this direction. In the pressure-driven case the boundary conditions are set to create a pressure gradient and no external field is applied, see Fig. 1.

The numerical solution of the compressible Navier-Stokes (NS) equations is obtained using a second-order Godunov method [14, 15, 16] to evaluate the hyperbolic fluxes and a Crank-Nicolson scheme to treat the parabolic terms, which are approximated by standard finite difference methods. The computation of the hyperbolic flux terms using the second-order Godunov procedure is an explicit procedure so that the integration algorithm has a time step restriction based on CFL considerations of the Euler equations. The implicit discretization of the parabolic terms requires the solution of a nonlinear system of equations and this is done by the standard Gauss-Seidel method.

Direct Simulation Monte Carlo (DSMC) [17] is a well-known algorithm for computing gas dynamics at the level of the Boltzmann equation. In DSMC, the state of the system is given by the positions and velocities of particles. In each time step, the particles are first moved as if they did not interact with each other. After moving the particles and imposing any boundary conditions, collisions are evaluated by a stochastic process, conserving momentum and energy and selecting the post-collision angles from their kinetic theory distributions. Being a stochastic algorithm, DSMC measurements have statistical variation but this variation is that of spontaneous fluctuations and so confidence intervals (error bars) may be evaluated using statistical mechanics. [18]

The boundary conditions for the Navier-Stokes equations are: at the entrance ($x = -L_x/2$),

$$\rho = \rho_0, \quad \partial \mathbf{v} / \partial x = 0, \quad p = p_+ \quad (9)$$

and at the exit ($x = L_x/2$),

$$\partial \rho / \partial x = 0, \quad \partial \mathbf{v} / \partial x = 0, \quad p = p_- \quad (10)$$

These boundary conditions were chosen in an effort to minimize the entrance and exit boundary layers, that is, mimic flow in a very long system. At the thermal walls ($y = \pm L_y/2$), the velocity and temperature boundary conditions are $\mathbf{v} = u_{slip} \hat{\mathbf{x}}$ and $T = T_0 + T_{jump}$, where the slip and jump corrections for a fully accommodating surface are [1]

$$u_{slip} = \alpha \lambda \frac{\partial u}{\partial y}, \quad T_{jump} = \beta \frac{2\gamma}{\gamma+1} \frac{\lambda}{Pr} \frac{\partial T}{\partial y}, \quad (11)$$

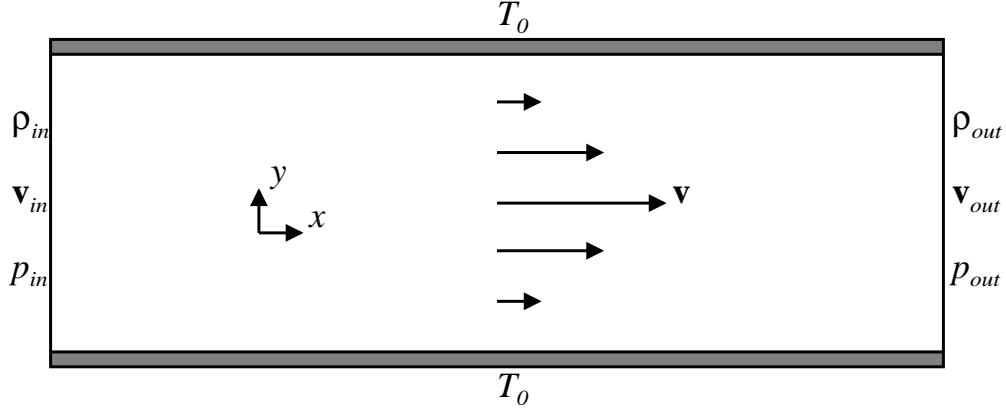


FIGURE 1. Pressure-driven Poiseuille flow

where λ is the mean free path, γ is the ratio of specific heats, and Pr is the Prandtl number. Ohwada et al. [19] and Sone et al. [20] predict the coefficients $\alpha = 1.11$ and $\beta = 1.13$, which is confirmed by DSMC simulations [21].

In the NS computation, the inflow boundary conditions are imposed by setting the values of the grid points at the entrance as,

$$\rho_{\text{in}} = \rho_0, \quad \mathbf{v}_{\text{in}} = \mathbf{v}_{\text{in}+1}, \quad p_{\text{in}} = p_+, \quad (12)$$

where $\mathbf{v}_{\text{in}+1}$ is the velocity at the grid point immediately to the right of an entrance grid point. The outflow boundary conditions at the exit are imposed in a similar fashion

$$\rho_{\text{out}} = \rho_{\text{out}-1}, \quad \mathbf{v}_{\text{out}} = \mathbf{v}_{\text{out}-1}, \quad p_{\text{out}} = p_-. \quad (13)$$

The inflow and outflow boundary conditions for DSMC are imposed by refreshing the particles in the cells at the entrance and exit as if they were in contact with a reservoir. At the entrance, the number of particles in each cell is set according to the boundary condition $\rho = \rho_0$. The individual particle velocities are generated according to the Chapman-Enskog distribution [22] with a temperature $T = mp_+/\rho k$ (perfect gas) and with a mean velocity equal to that of the adjacent fluid cell, $\mathbf{v}_{\text{in}+1}$. At the exit the number of particles in each cell is set equal to the number in the adjacent fluid cell so that $\partial\rho/\partial x = 0$; the particle velocities are set as at the entrance but using the exit pressure p_- . To minimize fluctuations the fluid velocity used in setting the entrance and exit boundary cells is evaluated as a running average.

NUMERICAL RESULTS

The simulated fluid is a hard sphere gas with particle mass $m = 1$ and diameter $d = 1$. At the reference density of $\rho_0 = 1.21 \times 10^{-3}$, the mean free path is $\lambda_0 = m(\sqrt{2}\pi\rho_0 d^2)^{-1} = 186$. The distance between the thermal walls is $L_y = 10\lambda_0$ and their temperature is $T_0 = 1$. The reference fluid speed is $u_0 = \sqrt{2kT_0/m} = 1$ so Boltzmann's constant is taken as $k = 1/2$. The reference sound speed is $c_0 = \sqrt{\gamma kT_0/m} = 0.91$ since $\gamma = 5/3$ for a monatomic gas. The reference pressure is $p_0 = \rho_0 kT_0/m = 6.05 \times 10^{-4}$. The acceleration and pressure gradient are chosen so that the flow will be sub-sonic, laminar and of similar magnitude in the two cases. Specifically, $\rho_0 f = 8.31 \times 10^{-8}$ for the acceleration-driven case and $dP/dx \approx 1.08 \times 10^{-7}$ for the pressure-driven case ($p_+ = \frac{3}{2}p_0$, $p_- = \frac{1}{2}p_0$, $L_x = 30\lambda_0$). In both cases the Knudsen number is $\text{Kn} = \lambda/L_y = 0.1$, the Mach number is $\text{Ma} \approx 0.5$ so the Reynolds number $\text{Re} \approx \text{Ma}/\text{Kn}$ is of order one.

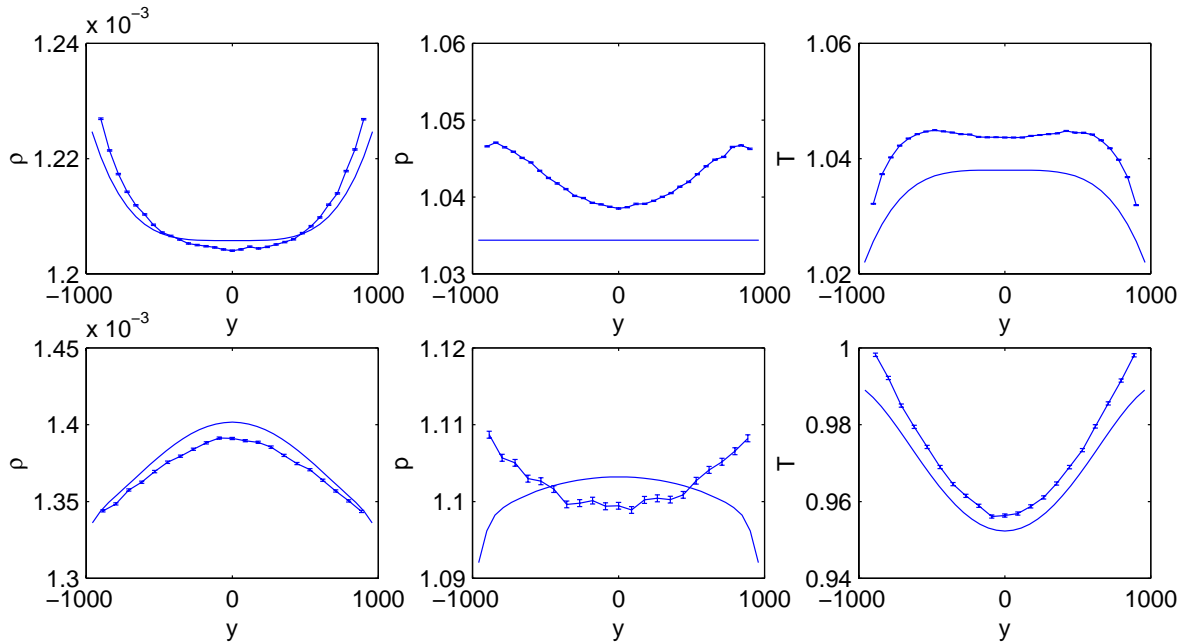


FIGURE 2. Stationary density, pressure, temperature profiles: the upper 3 plots are for the acceleration-driven case, the lower 3 plots are for the pressure-driven case in the cross-stream direction at the center of the system, the curves with error bars are the DSMC results; solid curves are NS results.

The code was first tested for the acceleration-driven case since, as described in the Introduction, this scenario has received considerable attention in the literature. The results, shown in Figures 2-6, upper plots, are in agreement with earlier studies and clearly show that the solution of the Navier-Stokes equations qualitatively does not match the DSMC measurement. Particularly, in DSMC one observes a non-constant pressure profile and a temperature dip in the center of the channel. Also, the pressure tensor profiles for components P_{xx} , P_{zz} and the heat flux profiles for component q_x differ from the solution of the Navier-Stokes equations. On the other hand, the Navier-Stokes equations do accurately predict the velocity profile, the pressure tensor profiles for diagonal component P_{yy} and all the off-diagonal components and the heat flux profiles for components q_y and q_z . These results are in agreement with earlier DSMC work [6], [9].

The results for the pressure-driven case are shown in Figures 2-7. The comparison with the acceleration-driven case is best made by considering the profiles in the cross-stream directions measured at the center of the system, Figures 2-6, lower part plots. As with the acceleration-driven case the Navier-Stokes equations are in qualitative agreement with the DSMC measurement for the velocity profile (Fig. 3) but unlike before the temperature profile (Fig. 2) is also in qualitative agreement. In the acceleration-driven case $T > T_0$ due to viscous heating but in the pressure-driven case $T < T_0$ since the viscous heating is surpassed by the expansion cooling. Interestingly, the DSMC data indicate a *reverse* temperature jump at the wall, that is, the temperature of the gas near the walls is slightly greater than T_0 though the temperature gradient normal to walls is negative. The NS and DSMC pressure profiles, pressure tensor components P_{xx} have opposite curvature (Fig. 2 and 4) but the magnitude of the pressure is nearly equal in the stream-wise direction (Fig. 7). The component P_{yy} qualitatively matches while P_{zz} is almost constant in DSMC, but has curvature in NS. The pressure tensor components P_{ij} match each other well. The heat flux profiles q_x shows the same curvature as NS in the center of the channel, but the profile is significant different near the thermal wall. The agreement for q_y and q_z is similar to the acceleration-driven case. The stream-wise velocity and temperature profiles (Fig. 7) do not agree as well as but this is not so surprising given that $\text{Kn} = 0.1$ and the aspect ratio is only $L_x/L_y = 3$.

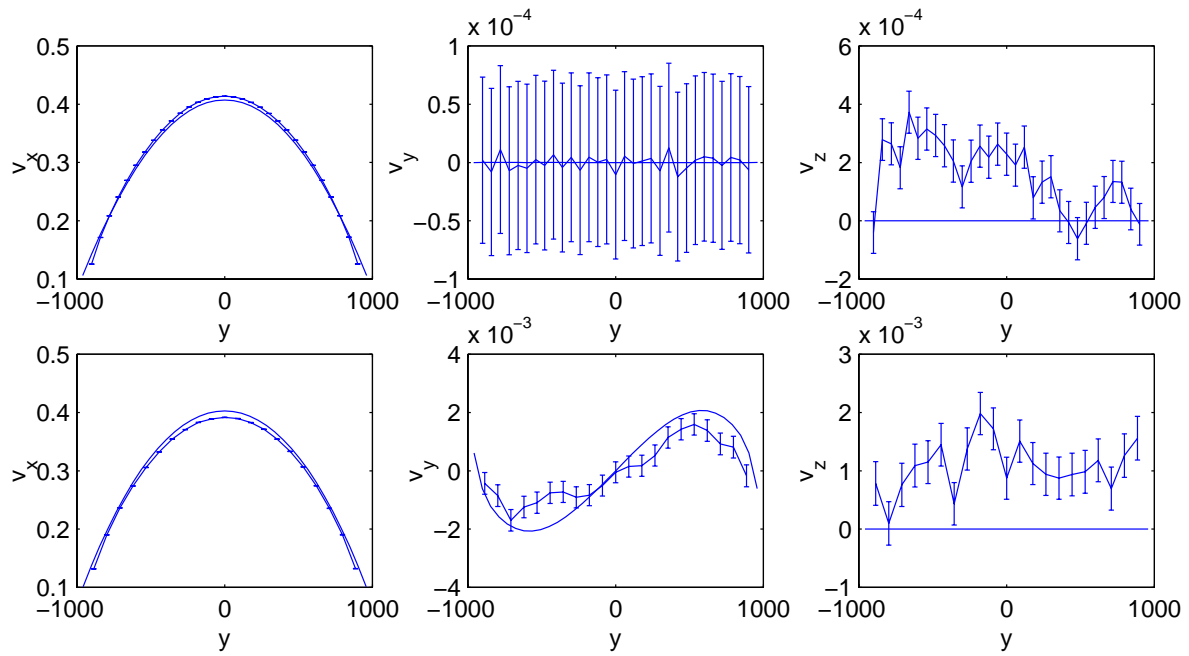


FIGURE 3. Stationary velocity profiles the upper 3 plots are for the acceleration-driven case, the lower 3 plots are for the pressure-driven case in the cross-stream direction at the center of the system, the curves with error bars are the DSMC results; solid curves are NS results.

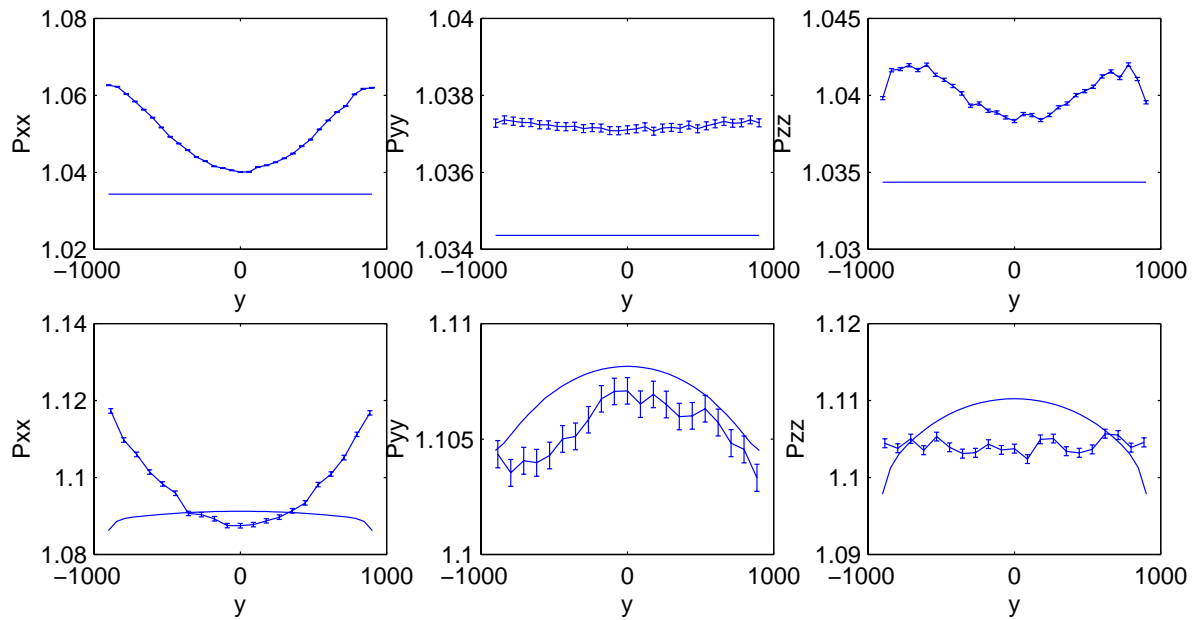


FIGURE 4. Stationary diagonal pressure tensor P_{ii} profiles the upper 3 plots are for the acceleration-driven case, the lower 3 plots are for the pressure-driven case in the cross-stream direction at the center of the system, the curves with error bars are the DSMC results; solid curves are NS results.

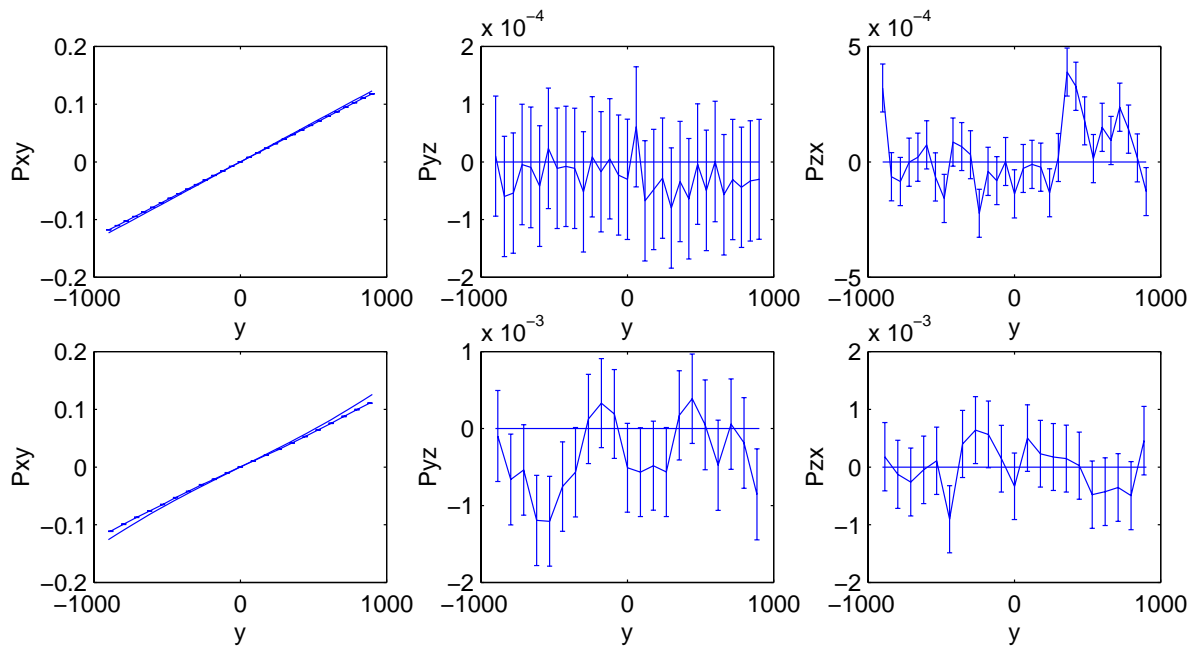


FIGURE 5. Stationary off-diagonal pressure tensor P_{ij} profiles: upper 3 plots are the acceleration-driven case, lower 3 plots are the pressure-driven case in the cross-stream direction at the center of the system, the curves with error bars are the DSMC results; solid curves are NS results.

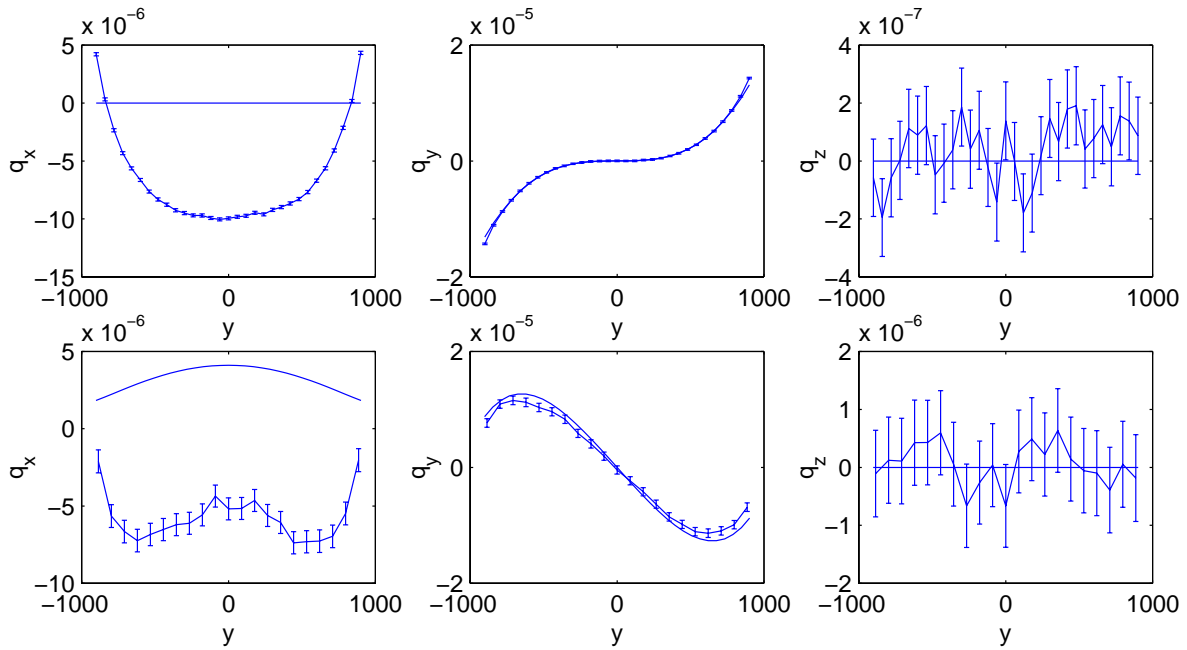


FIGURE 6. Stationary heat flux profiles: the upper 3 plots are for the acceleration-driven case, the lower 3 plots are for the pressure-driven case in the cross-stream direction at the center of the system, the curves with error bars are the DSMC results; solid curves are NS results.

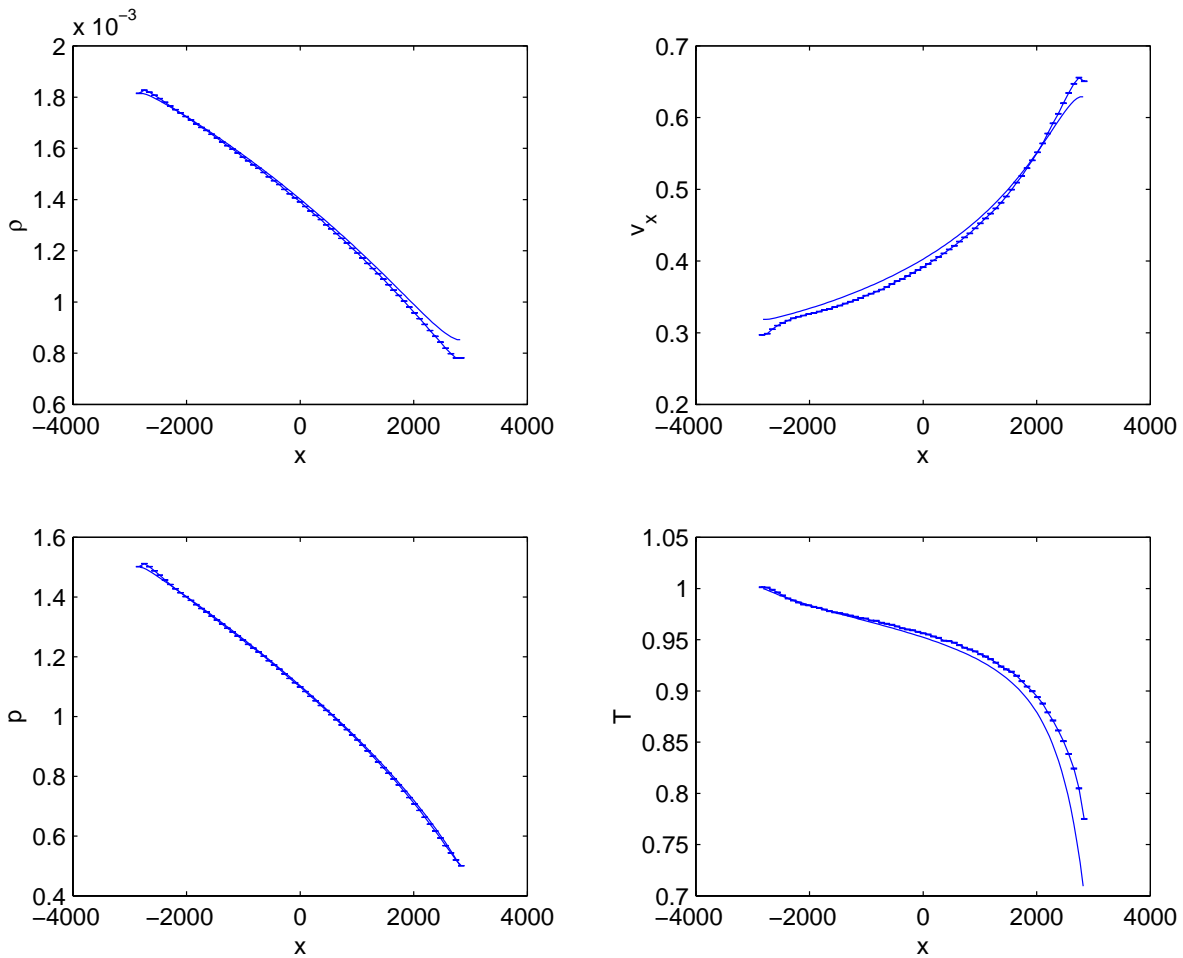


FIGURE 7. Stationary velocity, pressure and temperature profile for pressure-driven case; the curves with error bars are the DSMC results; solid curves are NS results. The profiles are in the stream-wise direction (x -direction) down the center-line ($y = 0$).

CONCLUSIONS

In this paper, plane Poiseuille flow is studied for acceleration-driven and pressure-driven conditions by comparing DSMC simulations with numerical solutions of the Navier-Stokes equations. In both acceleration and pressure-driven flows the velocity profile is approximately parabolic; the NS solution is in better agreement with the DSMC results in the former case. The qualitative difference observed in the temperature profile in the acceleration-driven case is not found in the pressure-driven case but the quantitative agreement is only fair. A concave pressure profile is observed in the DSMC data for both types of flow though NS give a strictly constant pressure in the acceleration-driven flow and a convex profile in the pressure-driven flow.

This investigation of pressure-driven Poiseuille flow is being extended in various directions. Some of the quantitative differences observed in the profiles are likely due to the influence of the entrance and exit conditions. These effects may be minimized by increasing the aspect ratio but then the pressure difference must be increased to maintain the same pressure gradient and the DSMC simulations become computationally more expensive. A better approach is to modify the entrance and exit reservoir conditions to better mimic the flow in a long channel. The quantitative and qualitative differences will also vary with Knudsen number, as has already been shown for acceleration-driven Poiseuille flow, and a similar analysis is underway for pressure-driven flow. Finally, the DSMC results will be compared with kinetic theory (BGK approximation, moment methods, etc.) in cases where predictions are available.

ACKNOWLEDGEMENTS

The authors wish to thank K. Aoki, G. Bird, N. Hadjiconstantinou, S. Hess, R. Hornung, M. Malek-Mansour, and S. Wijesinghe for helpful discussions. This work was performed under the auspices of the U.S. Department of Energy by University of California Lawrence Livermore National Laboratory under contract No. W-7405-Eng-48.

REFERENCES

1. C. Cercignani, *Boltzmann Equation and its Application*, Springer-Verlag, New York, (1988)
2. M. Mareschal, M.M. Mansour, A. Puhl and E. Kestemont, *Phys. Rev. Lett.* **61**:2550 (1988) A. Puhl, M.M. Mansour, and M. Mareschal, *Phys. Rev. A* **40**:1999 (1989)
3. J. Koplik, J.R. Banavar, *Ann. Rev. Fluid Mech.* **27**:257 (1995)
4. A. Santos, J.J. Brey, C.S. Kim and J.W. Dufty, *Phys. Rev. A*, **39**:320 (1989) C.S. Kim, J.W. Dufty, A. Santos and J.J. Brey, *Phys. Rev. A*, **40**:7165 (1989)
5. M. Tij and A. Santos, *J. Stat. Phys.*, **76**:1399 (1994)
6. M.M. Malek, F. Baras, and A.L. Garcia, *Physica A*, **240**:255 (1997)
7. M. Tij, M. Sabbane and A. Santos *Phys. Fluids*, **10**:1021 (1998)
8. D. Risso, P. Cordero, *Phys. Rev. E*, **58**:546 (1998)
9. F.J. Uribe and A.L. Garcia, *Phys. Rev. E*, **60**:4063 (1999)
10. S. Hess, M. Malek-Mansour, *Physica A*, **272**:481 (1999)
11. K. Aoki, S. Takata and T. Nakanishi, *Phys. Rev. E*, **65**:026315:1 (2002)
12. L. Landau and E. Lifshitz, *Fluid Mechanics*, Pergamon, London (1959)
13. J. C. Tannehill, D.A. Anderson and R. H. Pletcher, *Computational Fluid Mechanics and Heat Transfer* Taylor and Francis 1997
14. E. Toro, *Riemann solvers and numerical methods for fluid dynamics: a practical introduction* Springer-Verlag, Berlin; New York (1999)
15. C. Laney, *Computational Gasdynamics* Cambridge University Press, Cambridge New York, NY (1998)
16. M. Ben-Artzi and J. Falcovitz, *J. of Comp. Phys.* **55**:1 (1984)
17. G.A. Bird, *Molecular Gas Dynamics* Clarendon, Oxford, (1976); G.A. Bird, *Molecular Gas Dynamics and the Direct Simulation of Gas Flows* Clarendon, Oxford, (1994)
18. N. Hadjiconstantinou and A. Garcia, *Proceedings of the First MIT Conference on Computational Fluid and Solid Mechanics*, Elsevier, **1**:853 (2001).
19. T. Ohwada, Y. Sone, K. Aoki, *Phys. Fluids A* **1**:1588 (1989)
20. Y. Sone, T. Ohwada, K. Aoki, *Phys. Fluids A* **1**:363 (1988)
21. S. Wijesinghe, N. Hadjiconstantinou, *Proceedings of the First MIT conference on Computational Fluid and Solid Mechanics*, Elsevier, **2**:1019 (2001)
22. A. L. Garcia and B. J. Alder, *J. Comp. Phys.* **140**:66 (1998)